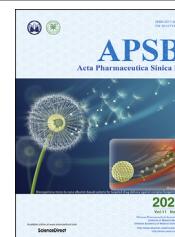




Chinese Pharmaceutical Association  
Institute of Materia Medica, Chinese Academy of Medical Sciences

Acta Pharmaceutica Sinica B

[www.elsevier.com/locate/apsb](http://www.elsevier.com/locate/apsb)  
[www.sciencedirect.com](http://www.sciencedirect.com)



ORIGINAL ARTICLE

# Cancer-specific calcium nanoregulator suppressing the generation and circulation of circulating tumor cell clusters for enhanced anti-metastasis combinational chemotherapy



Dan Li<sup>a</sup>, Yingli Wang<sup>a</sup>, Chang Li<sup>a</sup>, Qiu Wang<sup>a</sup>, Bingjun Sun<sup>a</sup>,  
Haotian Zhang<sup>b</sup>, Zhonggui He<sup>a</sup>, Jin Sun<sup>a,\*</sup>

<sup>a</sup>Department of Pharmaceutics, Wuyi College of Innovation, Shenyang Pharmaceutical University, Shenyang 110016, China

<sup>b</sup>School of Life Science and Biopharmaceutics, Shenyang Pharmaceutical University, Shenyang 110016, China

Received 11 March 2021; received in revised form 1 April 2021; accepted 12 April 2021

## KEY WORDS

Cell–cell junctions;  
Digoxin;  
Doxorubicin;  
Homologous targeting;  
Circulating tumor cell clusters;  
Epithelial–mesenchymal transition;  
Breast cancer;  
Lung metastasis

**Abstract** Tumor metastasis is responsible for chemotherapeutic failure and cancer-related death. Moreover, circulating tumor cell (CTC) clusters play a pivotal role in tumor metastasis. Herein, we develop cancer-specific calcium nanoregulators to suppress the generation and circulation of CTC clusters by cancer membrane-coated digoxin (DIG) and doxorubicin (DOX) co-encapsulated PLGA nanoparticles (CPDDs). CPDDs could precisely target the homologous primary tumor cells and CTC clusters in blood and lymphatic circulation. Intriguingly, CPDDs induce the accumulation of intracellular  $\text{Ca}^{2+}$  by inhibiting  $\text{Na}^+/\text{K}^+$ -ATPase, which help restrain cell–cell junctions to disaggregate CTC clusters. Meanwhile, CPDDs suppress the epithelial–mesenchymal transition (EMT) process, resulting in inhibiting tumor cells escape from the primary site. Moreover, the combination of DOX and DIG at a mass ratio of 5:1 synergistically induces the apoptosis of tumor cells. *In vitro* and *in vivo* results demonstrate that CPDDs not only effectively inhibit the generation and circulation of CTC clusters, but also precisely target and eliminate primary tumors. Our findings present a novel approach for anti-metastasis combinational chemotherapy.

**Abbreviations:** CI, combination index; CLSM, confocal laser scanning microscopy; CTC, circulating tumor cell; DAPI, 4',6-diamidino-2-phenylindole; DIG, digoxin; DiR, 1,1-dioctadecyl-3,3,3,3-tetramethylindotricarbocyanine iodide; DLS, dynamic light scattering; DOX, doxorubicin; EMT, epithelial–mesenchymal transition; H&E, hematoxylin and eosin; MMP-9, matrix metalloproteinase-9; MTT, 3-(4,5-dimethyl-2-thiazolyl)-2,5-diphenyl-2-*H*-tetrazolium bromide; TEM, transmission electron microscopy.

\*Corresponding author.

E-mail address: [sunjin@syphu.edu.cn](mailto:sunj@syphu.edu.cn) (Jin Sun).

Peer review under responsibility of Chinese Pharmaceutical Association and Institute of Materia Medica, Chinese Academy of Medical Sciences.

<https://doi.org/10.1016/j.apsb.2021.04.009>

2211-3835 © 2021 Chinese Pharmaceutical Association and Institute of Materia Medica, Chinese Academy of Medical Sciences. Production and hosting by Elsevier B.V. This is an open access article under the CC BY-NC-ND license (<http://creativecommons.org/licenses/by-nc-nd/4.0/>).

## 1. Introduction

Tumor metastasis occupies more than 90% of cancer-related mortality<sup>1</sup>. Metastasis is a complex process in which tumor cells can detach from the primary tumor by the epithelial–mesenchymal transition (EMT), then enter into the blood or lymphatic vessels as circulating tumor cells (CTCs) and spread into distant organs<sup>2,3</sup>. Chemotherapy is currently one of the main clinical treatment strategies for cancer. However, the latest research showed that the traditional chemotherapy could change the microenvironment of tumors and normal organs, and even promote tumor metastasis to a certain extent<sup>4–6</sup>. Moreover, CTCs are found in the blood and lymph as single CTCs and CTC clusters, and the metastatic capability of CTC clusters is 23–50 times higher than single CTCs<sup>7–9</sup>. Therefore, how to suppress the generation and circulation of CTC clusters is the key point for cancer anti-metastasis chemotherapy.

Digoxin (DIG) is an FDA-approved  $\text{Na}^+/\text{K}^+$ -ATPase inhibitor for the treatment of heart failure. DIG could suppress cell–cell junctions to disaggregate CTC clusters effectively<sup>10</sup> and cause the mitochondrial-mediated tumor apoptosis<sup>11,12</sup> by inhibiting  $\text{Na}^+/\text{K}^+$ -ATPase to elevate the intracellular  $\text{Ca}^{2+}$  concentration. Moreover, digoxin could also suppress the EMT process, further inhibiting the migration and invasion of breast cancer<sup>13,14</sup>. Thus, chemotherapy in combination with digoxin is expected to be more effective in the treatment of tumor anti-metastasis.

Our previous studies showed cell membrane coating nanotechnology could be effectively used to inhibit cancer metastasis by targeting CTCs and circulating tumor-derived exosomes<sup>15,16</sup>. Especially after coating with cancer membrane, nanoparticles had homologous targeting and immune escapement functions<sup>17–19</sup>. Compared with ligand–receptor targeting methods, homologous targeting could reduce the individual differences caused by tumor heterogeneity to a certain extent<sup>20</sup>. Therefore, cancer membrane-coated biomimetic nanoplatfoms could bypass the biological barrier, paving the way for an effective delivery system for precisely targeting primary tumor cells and CTC clusters.

In this study, cancer membrane-coated PLGA nanoparticles encapsulating digoxin (DIG) and doxorubicin (DOX) (CPDDs), namely cancer-specific calcium nanoregulators, were developed to effectively enhance anti-metastasis combinational chemotherapy. Remarkably, CPDDs had good homologous targeting capability, especially precisely targeting and disassembling CTC clusters in the blood and lymphatic circulation. CPDDs could cause mitochondrial-mediated apoptosis and disaggregate CTC clusters to inhibit tumor metastasis by up-regulating the intracellular  $\text{Ca}^{2+}$  concentration. Simultaneously, CPDDs further inhibited the formation of CTC clusters in the primary tumor by suppressing the EMT process. In summary, CPDDs inhibited tumor metastasis by suppressing CTC clusters generation and circulation, providing a novel strategy for anti-metastasis combination chemotherapy.

## 2. Material and methods

### 2.1. Materials

Digoxin, doxorubin, 1,1-dioctadecyl-3,3,3-tetramethylin dotricarbocycaineiodide (DiR), Fluo-4 AM, 3-(4,5-dimethylthiazol-2-yl)-2,5-diphenyl tetrazolium bromide (MTT) and 4',6-diamidino-2-phenylindole dihydrochloride (DAPI) were purchased from Dalian Meilun Biotech Co., Ltd. (Dalian, China). Mitochondrial Membrane Potential Assay Kit and Hoechst 33342 from Beijing Solarbio Science & Technology Co., Ltd. (Beijing, China). Cell culture reagents were bought from Gibco. All other agents and solvents were of analytical standard grade.

### 2.2. Preparation of CPDDs, CPDoS, CPDis and PDDs

Poly (lactic-*co*-glycolic acid) (PLGA) nanoparticles co-encapsulating DIG and DOX (PDDs) were prepared by an emulsion solvent evaporation method. Briefly, 30 mg PLGA, 0.5 mg DIG and 1 mg DOX were added to 2 mL mixture (dichloromethane: methanol = 4:1, *v/v*). Then, the solvent was added into 4 mL 1% PVA solution, sonicated at 400 W for 5 min in an ice bath, and stirred overnight. The particle suspensions were centrifuged at  $13,000\times g$  for 30 min.

The 4T1 cancer membrane (CM) was obtained using Membrane Protein Extraction Kit. The mixture of PDDs and CM was extruded through a 200 nm polycarbonate membrane for at least 5 cycles. The same preparation method was also applied in CPDoS or CPDis.

### 2.3. Characterization of CPDDs, CPDoS, CPDis and PDDs

The particle size, zeta potential and morphology of nanoparticles were measured using dynamic light scattering (DLS) examination (Malvern, Nano ZS, UK) and transmission electron microscopy (TEM, Hitachi, HT7700, Japan), respectively. The drug encapsulation efficiency was measured by HPLC (Waters, C18 column, 5  $\mu\text{m}$ , 4.6 mm  $\times$  250 mm, USA) using methanol and pH 3.5 ammonium phosphate buffer as the elute.

### 2.4. In vitro drug release

The DOX and DIG release from PDDs and CPDDs were measured by dialysis method at 37 °C in PBS with 30% ethanol. In brief, the dialysis tubes (MWCO = 3.5 kDa) containing 1 mL PDDs or CPDDs were immersed into 30 mL PBS and shaken at 100 rpm. 1 mL medium was taken out and replaced with 1 mL fresh medium at the pre-determined time point. Then, drug concentration was determined using HPLC analysis.

### 2.5. Cell culture and animals

Mouse macrophage RAW264.7 cells and 4T1 mouse breast carcinoma cells were cultured with RPMI 1640 medium supplemented with streptomycin (100 µg/mL), penicillin (100 units/mL) and 10% FBS. Mouse fibroblast 3T3 cells were maintained in DME/F12 as described above. All cells were incubated in a humidified atmosphere of 5% CO<sub>2</sub> at 37 °C.

All experimental procedures were executed according to the protocols approved by Shenyang Pharmaceutical University Animal Care and Use Committee, Shenyang, China.

### 2.6. Western blotting for membrane proteins in CM, CPD<sub>os</sub>, CPD<sub>is</sub>, CPDD<sub>s</sub>

Proteins were quantified using the BCA Protein Assay Kit (Dingguo, China), and then the same amount of protein samples were added to SDS-PAGE to separate proteins, followed by Coomassie blue staining. The proteins were transferred to PVDF membrane (Bio-Rad, USA), blocked with 5% skim milk for 1 h and incubated with the primary antibodies and followed by the secondary antibodies for 1 h at room temperature before imaging with ECL Western Blotting Substrate (Solarbio, China).

### 2.7. Cytotoxicity assays

The MTT method was used to determine the cytotoxicity of PDDs, CPD<sub>os</sub>, CPD<sub>is</sub> and CPDD<sub>s</sub> against 4T1 cells. A 96-well plate was seeded 2000 cells per well for 12 h, and serial dilutions of different formulations were added. After 48 h, 20 µL MTT solution (5 mg/mL in distilled water) was added at 37 °C for 4 h. Afterwards, the medium was discarded and replaced with 150 µL DMSO. The absorbance was measured at 570 nm.

### 2.8. In vitro targeting and macrophages phagocytosis

4T1, 3T3, and RAW264.7 cells ( $5 \times 10^4$  cells) were seeded in a 12-well plate for 12 h. PDDs and CPDDs (DOX 5 µg/mL, DIG 1 µg/mL) were then added to the cells for 4 h. Subsequently, the culture medium was discarded, and the cells were washed, fixed, and stained with Hoechst 33342 for 10 min. DOX fluorescence signals were collected by a confocal laser scanning microscope (CLSM, Nikon C2, Japan) and quantified by FACSCalibur flow cytometry.

### 2.9. Cell migration and invasion assays

Transwell assays were utilized to assess the inhibition of CPDDs on the migration and invasion activities. For the migration assays, 100 µL FBS-free RPMI 1640 media ( $2 \times 10^5$  4T1 cells) were added to the top chambers of inserts. For the invasion assays, the upper chambers of inserts were pre-coated with 20 µL Matrigel matrix (BD, USA), and added 100 µL of  $2 \times 10^5$  4T1 cells in FBS-free media. Then, the RPMI-1640 medium containing 10% FBS was added to the lower chamber. The cells were treated with CPDDs, CPD<sub>os</sub>, CPD<sub>is</sub>, PDDs and DD (DOX 1 µg/mL, DIG 0.2 µg/mL) for 24 h. The migrated or invaded cells through the Transwells were stained with violet crystal and counted to calculate the inhibitory rate. The cells without any treatment served as the control.

### 2.10. Mechanism study of metastasis

Ca<sup>2+</sup> changes were detected via Fluo-4 AM. 4T1 cells were treated with CPD<sub>os</sub>, CPD<sub>is</sub> or CPDD<sub>s</sub>. The cells were stained with Fluo-4 AM and MitoRed probe. Ca<sup>2+</sup> changes were visualized by using CLSM (Japan).

Cell clusters size changes were detected after CPDDs incubation. 4 mL 4T1 cells ( $1 \times 10^5$  cells/mL) suspension was seeded into the flask, then placed on a shaking table concentrator (37 °C, 60 rpm)<sup>21</sup>. After 2 h, CPD<sub>os</sub>, CPD<sub>is</sub>, CPDD<sub>s</sub> were added for 4 h, then the cells were washed and fixed. Finally, randomly selected five fields to be imaged by a microscope at 20 × magnification, and the mean CTC cluster size in each field was counted.

Western blot analysis was employed to study the changes of N-cadherin, vimentin and matrix metalloproteinase-9 (MMP9) in 4T1 cells treated with CPD<sub>os</sub>, CPD<sub>is</sub> and CPDD<sub>s</sub>. Subsequently, the changes in the concentration of N-cadherin, vimentin and MMP9 in the above cell lysates were analyzed.

### 2.11. Mechanism study of cell apoptosis

Western blot analysis was employed to study the changes of caspase-3, cytochrome *c* and BCL-2. The changes of cleaved caspase-3, cytochrome *c* and BCL-2 in the cell lysates were analyzed.

Mitochondrial membrane potential changes were detected by JC-1 kit. The 4T1 cells were seeded in a 12-well plate and cultured for 12 h. The cells were treated with CPD<sub>os</sub>, CPD<sub>is</sub> and CPDD<sub>s</sub>. After incubation, cells were stained for 30 min. Mitochondrial membrane potential changes were observed using CLSM.

### 2.12. Studies on 4T1 orthotopic breast tumor models

The 4T1 orthotopic breast tumor model was used to evaluate the biological distribution of CPDDs. 50 µL PBS containing 4T1 cells ( $1 \times 10^6$  cells) were injected into the left side of the fourth fat pad of female BALB/c mice. When the tumor reached approximately 200 mm<sup>3</sup>, 100 µL DiR-loaded PDDs and CPDDs (DiR 1 mg/kg) were intravenously injected. NIRF images *in vivo* were acquired by the IVIS system at 0.5, 2, 6, 12, and 24 h after injection. After 12 h injection, major organs and tumors were collected for analysis.

50 µL PBS containing 4T1 cells ( $1 \times 10^6$  cells) were inoculated to the left of the fourth fat pad of female BALB/c mice. After 10 days, the average tumor volume reached about 75 mm<sup>3</sup>. Mice were randomly divided into six groups: control (saline), CPDDs, CPD<sub>os</sub>, CPD<sub>is</sub>, PDDs and DD. These preparations were intravenously administered every other day (DOX 2 mg/kg, DIG 0.4 mg/kg) for a total of four injections. Tumor volume and weight were measured daily. At the end of 15 treatment days, all mice were sacrificed. Blood was then collected for measurement of liver and kidney function markers and the whole lungs were stained by Bouin's. Major organs and tumors were isolated, weighed and sectioned for hematoxylin and eosin (H&E) staining and TUNEL immunofluorescence staining.

### 2.13. Studies on lymphatic metastasis model

The foot soles of 4T1 tumor-bearing model were used to evaluate the ability of CPDDs to track CTC clusters from the lymphatic circulation. As mentioned in the previous report, 20 µL PBS

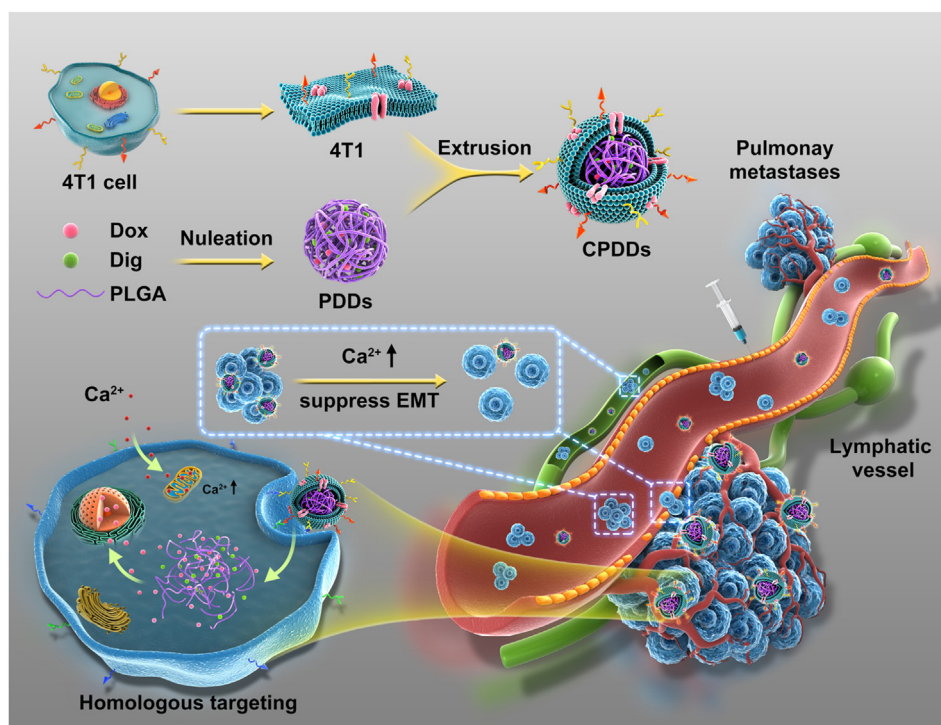


**Figure 1** Schematic illustration of cancer-specific calcium nanoregulator for enhancing anti-metastasis combinational chemotherapy by targeting the homologous tumor cells, restraining the EMT, dissociating and depleting CTC clusters. CTC, circulating tumor cell; CPDDs, cancer membrane-coated digoxin and doxorubicin co-encapsulated PLGA nanoparticles; DIG, digoxin; DOX, doxorubicin; EMT, epithelial–mesenchymal transition.

containing 4T1 cells ( $1 \times 10^6$  cells) were injected into the left hind foot soles of female BALB/c mice<sup>22</sup>. When the tumor reached about 200 mm<sup>3</sup>, 50  $\mu$ L DiR-loaded PDDs and CPDDs (DiR 1 mg/kg) were intratumorally injected. NIRF images *in vivo* were acquired by the IVIS system at 20 min, 1, 2, 6 and 12 h after injection.

The foot soles of 4T1 tumor-bearing models were used to evaluate the lymphatic anti-metastasis effects of CPDDs *in vivo*. 20  $\mu$ L PBS containing 4T1 cells ( $1 \times 10^6$  cells) were inoculated to the left hind foot soles of female BALB/c mice. After 10 days, the average tumor reached approximately 75 mm<sup>3</sup>. Mice were randomly divided into six groups: saline, CPDDs, CPDoS, CPDiS, PDDs and DD. These preparations were intratumorally administered every other day (DOX 2 mg/kg, DIG 0.4 mg/kg) for a total of four injections. Weight was measured daily. After 14 treatment days, all mice were killed. The whole lungs were stained and the lymph node volume was measured. Liver and lung were isolated and sectioned for H&E staining.

#### 2.14. Studies on CTC clusters metastasis model

Luc-4T1 cell clusters were intravenously injected into the BALB/c mice, which were randomly divided into two groups. 100  $\mu$ L DiR-loaded PDDs and CPDDs were intravenously injected, respectively. *Ex vivo* images of main organs at 12 h were acquired by the IVIS system. Additionally, lung metastasis luminescent signals were monitored by luminescent signals.

4T1 cell clusters ( $2 \times 10^5$  cells) were intravenously injected into the BALB/c mice (18–22 g), and randomly divided into six groups. At 2 h and Days 2, 4, 6 after the inoculation, saline, CPDDs, CPDoS, CPDiS, PDDs and DD (DOX 2 mg/kg, DIG

0.4 mg/kg) were respectively injected to these animals. On Day 14, mice were sacrificed and lungs were stained with Bouin's. Liver and lung of different groups were isolated and sectioned for H&E staining.

#### 2.15. Statistical analysis

The mean  $\pm$  SD were calculated for all data. Significant differences were analyzed by Student's *t*-test (\* $P < 0.05$ , \*\* $P < 0.01$ , \*\*\* $P < 0.001$  and \*\*\*\* $P < 0.0001$ ).

### 3. Results and discussion

#### 3.1. Design, preparation and characterization of CPDDs

PLGA nanoparticles co-encapsulating DIG and DOX were prepared by an emulsion solvent evaporation method, named as PDDs<sup>16</sup>. Then, CM derived from 4T1 breast cancer cell membranes was obtained, and co-extruded with PDDs to obtain CPDDs (Fig. 1). Besides, CM-coated PLGA nanoparticles encapsulating DOX- or DIG-single were also prepared as the control, named as CPDoS and CPDiS respectively. We firstly investigated the anti-metastatic capacity of CPDDs with different DOX/DIG ratios using CTC clusters metastasis model. It was found that the DOX/DIG ratio of 5:1 exhibited the best anti-metastatic effect, and this ratio was used for subsequent studies (Supporting Information Fig. S1). PDDs and CPDDs had regular spherical shapes (Fig. 2A). Compared with PDDs, the zeta potential of CPDDs decreased from  $-4$  to  $-18$  mV, and the average particle size increased by about 40 nm (Fig. 2B). These results indicated the PDDs were successfully coated with CM. The

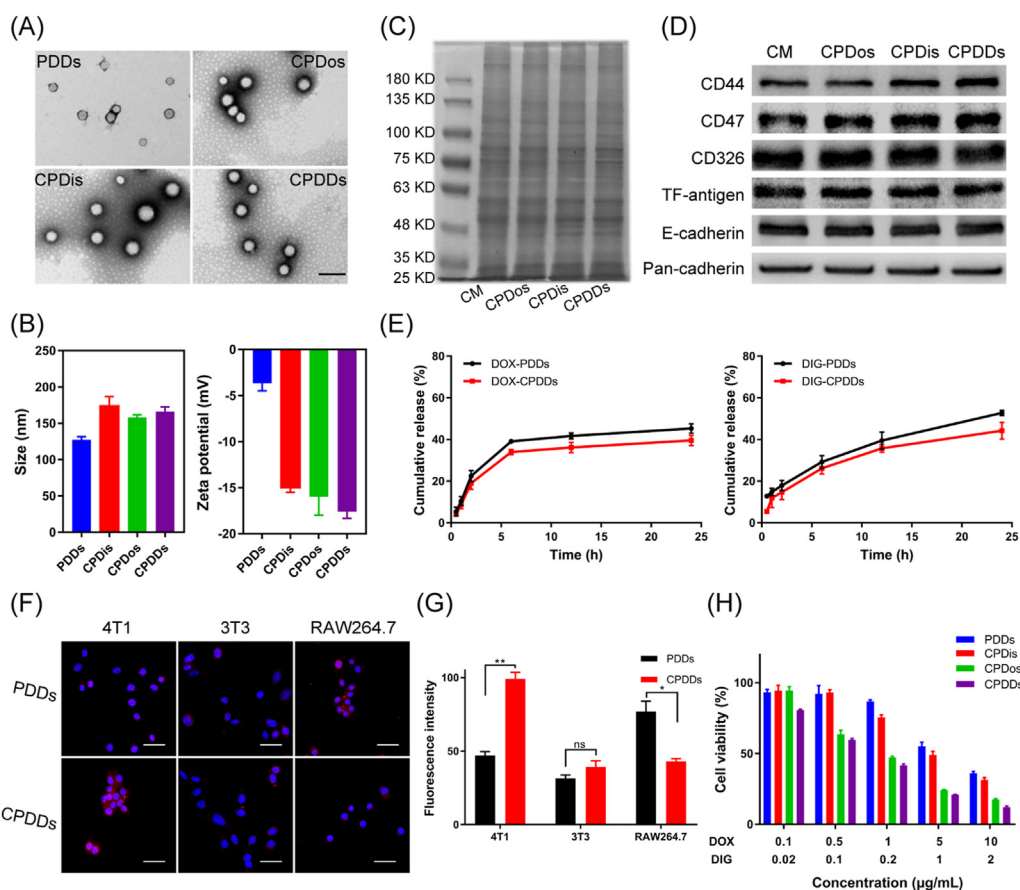


**Figure 2** Characteristics of cancer-biomimetic nanoparticles. (A) TEM images of PDDs, CPDos, CPDis and CPDDs. Scale bar = 200 nm. (B) Hydrodynamic diameter and zeta potential of PDDs, CPDos, CPDis and CPDDs. (C) SDS-PAGE protein analysis of CM, CPDos, CPDis and CPDDs. (D) Western blotting of CM, CPDos, CPDis and CPDDs. Pan-cadherin was used as a control. (E) Drug release of DIG and DOX from PDDs and CPDDs. (F) Intracellular uptake of CPDDs in 4T1, 3T3 and RAW264.7 cells. Scale bar: 20  $\mu$ m. (G) DOX fluorescence intensity measured by flow cytometry. (H) *In vitro* cytotoxicity against 4T1 cells with different concentrations. Data are presented as mean  $\pm$  SD ( $n = 3$ ); \* $P < 0.05$ , \*\* $P < 0.01$ , ns, not significant.

encapsulation efficiencies of DOX and DIG in CPDDs were 84.9% and 31.6%, respectively.

According to previous reports, SDS-PAGE and Western blotting assay were performed to verify the expression of CPDDs membrane proteins<sup>17,23</sup>. SDS-PAGE results showed good preservation of the CM proteins in the protein profile of CPDDs in Fig. 2C. Five unique membrane proteins including CD44, CD326, CD47, TF-antigen and E-cadherin, were confirmed, because they all play vital roles during the tumor metastasis process. TF-antigen and E-cadherin are related to the adhesion abilities in the process of colonization of metastasis, and also affect the homologous interactions among tumor cells<sup>24,25</sup>. CD44 and CD326 play key roles in the adhesion of CTC clusters to metastasis<sup>26,27</sup>. CD47 is related to tumor invasion and decreased uptake by macrophages<sup>28</sup>. As shown in Fig. 2D, they were all well-preserved on the cancer-biomimetic nanoparticles, indicating that CPDDs could precisely target homologous tumor cells and escape macrophage phagocytosis.

Fig. 2E showed that drug release from PDDs was slightly delayed by coating with CM. Less than 40% and 45% of DOX and DIG were released from CPDDs, while over 45% and 50% of DOX and DIG were released from PDDs within 24 h, respectively. This may be due to the outer membrane acting as a diffusion barrier to prevent drug release.

### 3.2. Cellular uptake and cytotoxicity

To verify the homologous targeting capabilities of CPDDs, the intracellular uptake of CPDDs was studied in 4T1 and 3T3 cells. As depicted in Fig. 2F, the intensity of PDDs in 4T1 cells was notably lower than CPDDs, indicating the coating of homologous cytomembranes could improve the cellular uptake efficiency. Moreover, the fluorescence intensity of CPDDs in 4T1 cells was 2.6-fold higher than that in 3T3 cells in Fig. 2G, implying that the cancer-biomimetic nanoparticles had the selective affinity for homologous cancer cells as observed in other reports<sup>29–31</sup>. Furthermore, we investigated the escaping ability of CPDDs and PDDs from macrophage phagocytosis. The fluorescence signal of PDDs in RAW264.7 was 1.8-fold higher than that of CPDDs (Fig. 2G), indicating that CPDDs could effectively inhibit macrophage phagocytosis. Subsequently, the cytotoxicity of different groups was evaluated by MTT assay. The  $IC_{50}$  value of CPDDs was 0.74  $\mu$ g/mL (DOX dose) and the combination index (CI) was 0.69 in 48 h, suggesting that CPDDs had good synergistic effect (Fig. 2H). Besides, the  $IC_{50}$  value of CPDDs was 8-fold lower than that of PDDs, resulting from the higher intracellular uptake of CPDDs in 4T1 cells than that of PDDs.

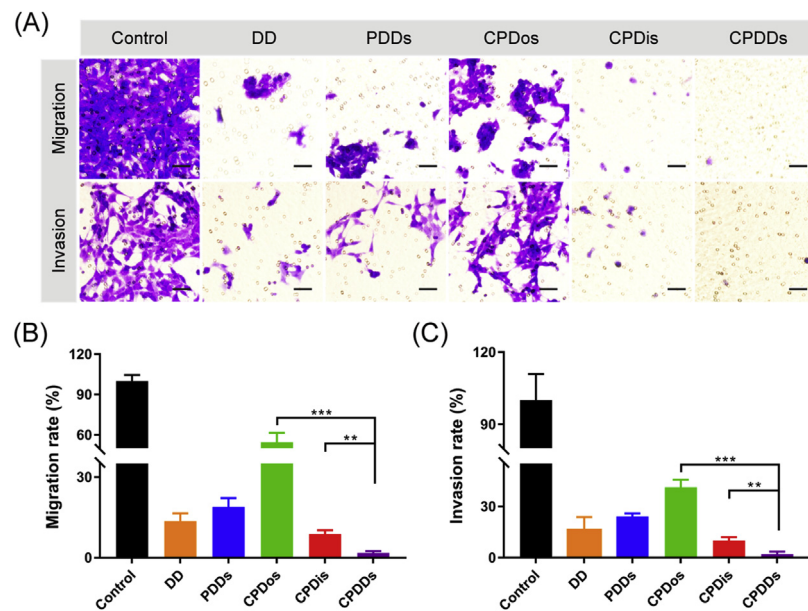


**Figure 3** Inhibition of CPDDs on the 4T1 cells migration and invasion. (A) Photographs of migrating or invading cells across the Transwell membrane. Migrating or invading cells were represented in the captured images as violet regions. Scale bar = 50  $\mu\text{m}$ . (B) The percentage of migrating cells compared to the control. (C) The percentage of invading cells compared to the control. Data are presented as mean  $\pm$  SD ( $n = 3$ ); \*\* $P < 0.01$ , \*\*\* $P < 0.001$ .

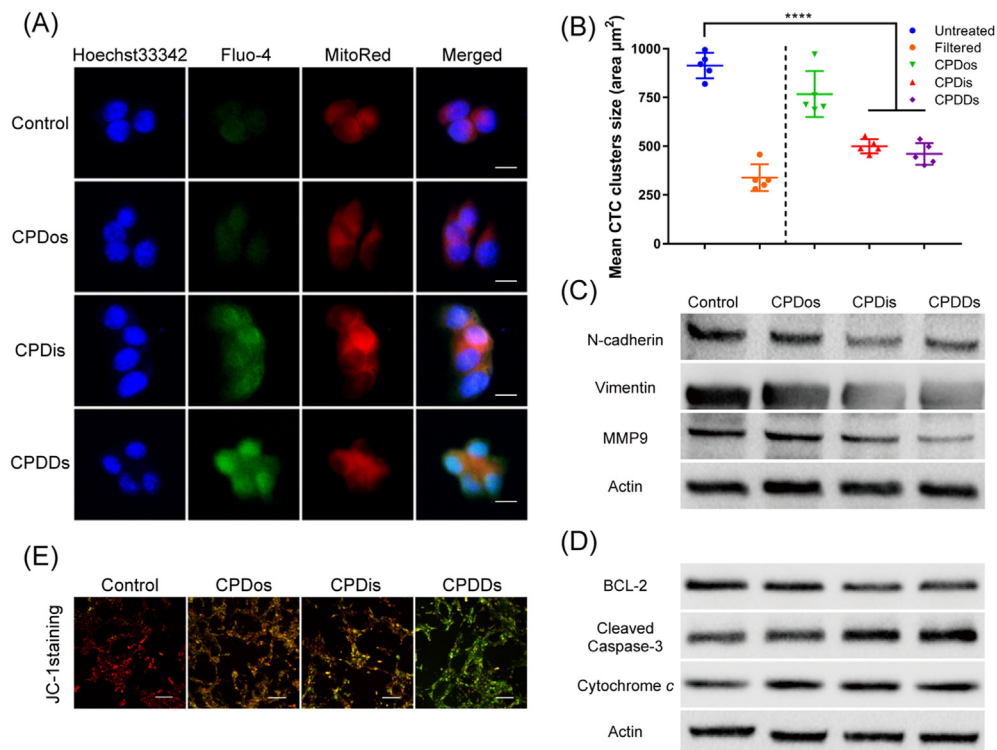


**Figure 4** Mechanism study of metastasis and cell apoptosis. (A) Intracellular  $\text{Ca}^{2+}$  changes after treatment with CPDos, CPDis and CPDDs in 4T1 cells. Scale bar: 5  $\mu\text{m}$ . (B) The mean CTC clusters size with different groups ( $n = 5$ ). 4T1 cell clusters that were 40 mm filtered (orange) or untreated (blue) are depicted as controls. (C) Western blot assays of N-cadherin, vimentin and MMP9. Actin was used as a control. (D) Western blot of BCL-2, cleaved caspase-3, and cytochrome c. Actin was used as a control. (E) Changes in mitochondria membrane potential of 4T1 cells by JC-1 staining. Scale bar = 50  $\mu\text{m}$ .

### 3.3. Inhibition of CPDDs on the migration and invasion activities

The inhibition of DD (free DOX and DIG solution), PDDs, CPDIs, CPDIs and CPDDs on 4T1 cells migration and invasion were determined by Transwell assays. Cell migration and invasion are two basic steps in the process of cancer metastasis<sup>32,33</sup>. Migrating or invading cells were represented in the captured images as violet regions. Migrating or invading cells were widely detected in the control group, suggesting that 4T1 cells had high metastatic activity. Similarly, CPDIs showed a limited inhibitory effect, while CPDDs inhibited the migration and invasion to the maximum extent (Fig. 3A). In comparison with the control, the migrating cells of the CPDDs were reduced by 98.2% (Fig. 3B), while the invading cells across the Matrigel-coated membrane were significantly reduced by 97.9% (Fig. 3C). Therefore, CPDDs could

remarkably suppress the migration and invasion activity, indicating great potential for anti-metastasis efficacy.

### 3.4. Mechanism study of metastasis and cell apoptosis

To clarify the anti-metastasis mechanism, the expression of crucial molecules related to tumor metastasis and the effects of CPDDs on  $Ca^{2+}$  levels were investigated. Previous studies had clearly demonstrated the ability of  $Na^+/K^+-ATPase$  inhibitor to disaggregate CTC clusters by regulating  $Ca^{2+}$  concentration<sup>10</sup>. As depicted in Fig. 4A and B, CPDIs and CPDDs significantly increased the intracellular  $Ca^{2+}$  to disaggregate tumor cell clusters. From a high-magnification Bio-TEM image (Supporting Information Fig. S2), CPDDs could restrain cell–cell junctions. Meanwhile, DIG also could inhibit the EMT by down-regulating N-cadherin, vimentin and matrix metalloproteinase-9 (MMP9),

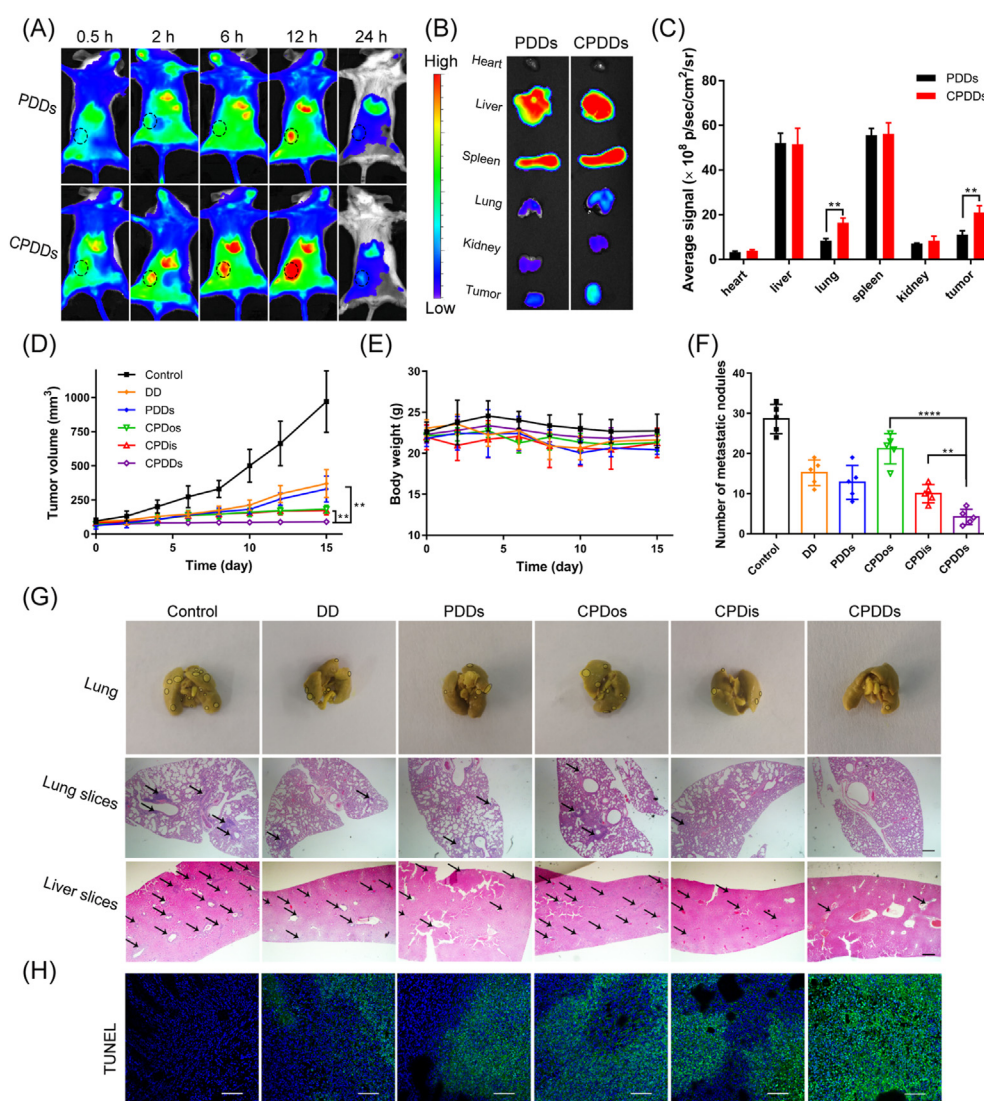


**Figure 5** *In vivo* anti-tumor and anti-metastasis effects of CPDDs on 4T1 orthotopic breast tumor-bearing models. (A) *In vivo* fluorescence imaging at 0.5, 2, 6, 12 and 24 h after injection with PDDs and CPDDs. Black circles demonstrate tumor tissues. (B) *In vitro* fluorescence imaging and (C) Fluorescent intensities analysis of normal tissues and tumors after 12 h injection. (D) Tumor-growth profiles. (E) Body weight changes. (F) Quantitative analysis of pulmonary metastatic nodules. (G) Photographs of Bouin's staining for lungs and H&E staining for lung and liver slices after treatment. Black circles show metastatic sites. Black arrows demonstrate metastatic nodules. Scale bar = 200  $\mu$ m. (H) TUNEL staining of tumor tissues. Scale bar = 50  $\mu$ m. Data are presented as mean  $\pm$  SD ( $n = 5$ ); \*\* $P < 0.01$ , \*\*\*\* $P < 0.0001$ .

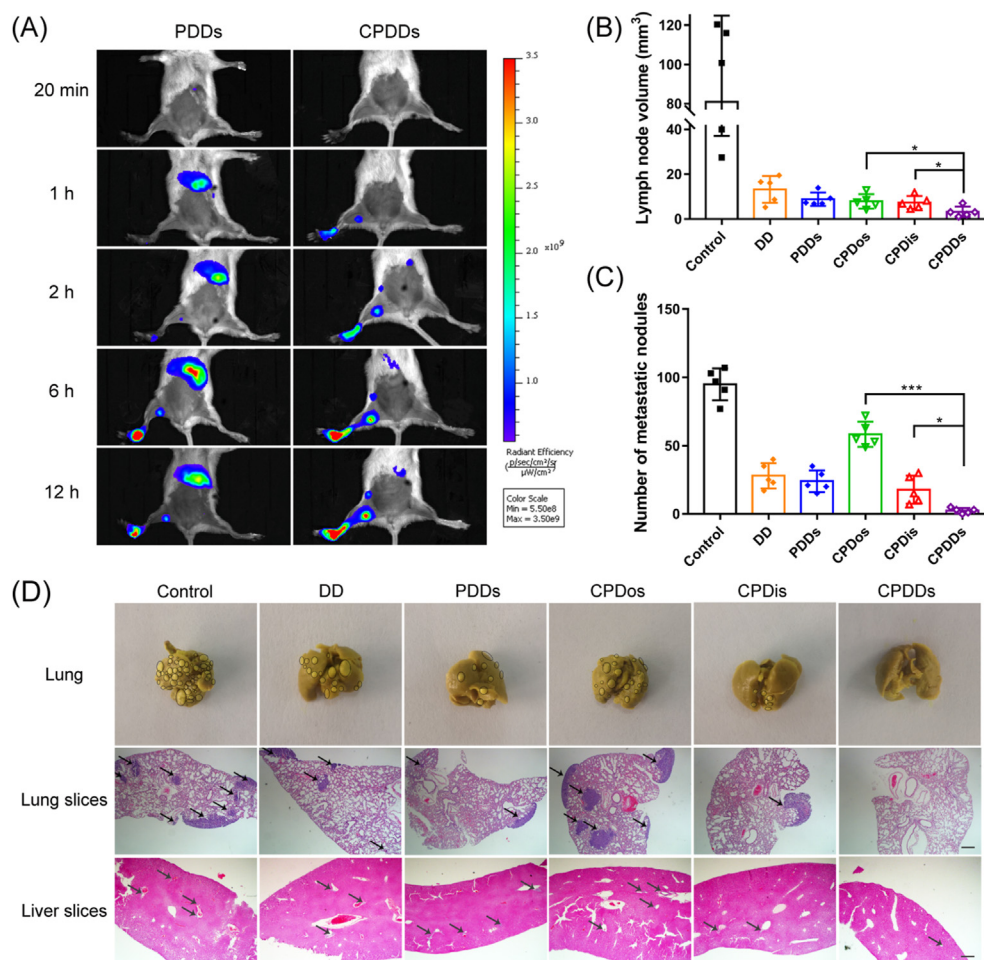


**Figure 6** *In vivo* anti-metastasis treatment on lymphatic and CTC clusters metastasis model. (A) *In vivo* fluorescence imaging at 20 min, 1, 2, 6 and 12 h after intratumoral injection with PDDs and CPDDs. (B) Volume of lymph node. (C) Quantitative analysis of pulmonary metastatic nodules on CTC clusters metastasis model. (D) Photos of Bouin's staining for lungs and H&E staining for lung and liver slices after treatment on CTC clusters metastasis model. Black circles show the metastatic sites. Black arrows demonstrate metastatic nodules. Scale bar = 200  $\mu\text{m}$ . Data are presented as mean  $\pm$  SD ( $n = 5$ ); \* $P < 0.05$ , \*\*\* $P < 0.001$ .

thereby suppressing cancer migration and invasion<sup>34–36</sup>. Compared with the control, CPDis and CPDDs suppressed EMT by down-regulating N-cadherin, vimentin and MMP9 (Fig. 4C), further confirming that DIG had a good anti-metastasis effect. Therefore, CPDDs could inhibit tumor metastasis both from the generation and circulation of CTC clusters.

Besides, it showed that a large amount of  $\text{Ca}^{2+}$  flowed into mitochondria (Fig. 4A). Therefore, we further investigated the effect of CPDDs on the mitochondrial  $\text{Ca}^{2+}$  homeostasis-related apoptosis. Mitochondrial membrane potential changes were measured by JC-1 kit. The cells exhibited almost red fluorescence in the control, indicating a relatively high mitochondrial membrane potential. As depicted in Fig. 4E, more green fluorescence was shown in the CPDDs, indicating that CPDDs could induce the unbalance of mitochondrial  $\text{Ca}^{2+}$  homeostasis. Subsequently, the effects of CPDDs on BCL-2, caspase-3 and cytochrome *c* were explored by Western blotting. The inhibition of BCL-2 induced cytochrome *c* release from the mitochondria in the process of triggering cell apoptosis by caspase-3 activation<sup>37</sup>. Caspase-3 was obviously activated, BCL-2 was down-regulated and the expression of cytochrome *c* increased in CPDDs group, suggesting the initiation of mitochondria-mediated apoptosis pathway (Fig. 4D).

### 3.5. Studies on 4T1 orthotopic breast tumor-bearing models

To investigate whether the CPDDs could specifically target tumor, DiR-loaded PDDs and CPDDs were injected into 4T1 orthotopic breast tumor-bearing mice *via* tail vein, respectively. Lung metastasis was confirmed by Bouin's staining (Supporting Information Fig. S3). The fluorescence signals of CPDDs in lung and tumor tissue were 2.0- and 1.9-fold higher than PDDs, respectively (Fig. 5B and C). The tumor fluorescence intensity was increased until 12 h after injection (Fig. 5A). Meanwhile, the *ex vivo* bioluminescent images confirmed the successful modeling of lung metastasis (Supporting Information Fig. S7A) and the *ex vivo* fluorescent images demonstrated that CPDDs have significantly higher lung metastasis-targeting effect than PDDs at 12 h after administration in CTC clusters metastasis model (Fig. S7B). It revealed that CPDDs had excellent active targeting ability to lung metastasis and tumor.

The anti-tumor and anti-metastasis effects were further evaluated in 4T1 orthotopic breast tumor-bearing mice. The tumor volume increased significantly from the initial  $\sim 75$ – $\sim 970$  mm<sup>3</sup> in the control group. Compared with the control, CPDDs significantly mitigated rapid tumor growth, while both CPDDs and

CPDDs showed partial inhibitory effects (Fig. 5D). Moreover, the severest tumor apoptosis in TUNEL staining tumor sections was observed in CPDDs group (Fig. 5H), indicating the CPDDs exhibited the highest anti-tumor growth efficacy. Meanwhile, all groups had no significant systemic toxicity in terms of H&E staining sections, body weight, liver and kidney function (Fig. 5E, Supporting Information Figs. S4 and S5).

To verify the anti-metastasis effect of CPDDs, H&E staining sections and Bouin's staining of the entire lung tissue were examined. In comparison with the control, the number of metastatic nodules in the CPDDs was slightly reduced, but significantly decreased in the CPDDs, indicating that DIG played a key role in anti-metastasis. Surprisingly, treatment with CPDDs further inhibited metastasis, with only 14.7% of the number of metastatic nodules in the control (Fig. 5F and G). Altogether, CPDDs could effectively suppress the growth and metastasis of 4T1 primary tumor.

### 3.6. Studies on the lymphatic and CTC clusters metastasis models

We finally examined whether the CPDDs could target CTC clusters in the lymphatic and CTC clusters metastasis models. The foot soles of 4T1 tumor-bearing models were used to evaluate the ability of CPDDs to track CTC clusters from the lymphatic circulation, with PDDs as a negative control. Compared with PDDs after injection, CPDDs moved to adjacent sentinel lymph node 1 h later, and spread to the next level of subiliac lymph node 2 h later (Fig. 6A), revealing that CPDDs could penetrate deeper into the lymph nodes to track CTC clusters. Furthermore, the sentinel lymph node volume of the control group (saline) was larger than that of the CPDDs group. CPDDs group also showed much smaller lymph node volume than CPDDs and CPDDs (Fig. 6B). Simultaneously, as shown in H&E staining and Bouin's staining of liver and lung sections, there were no significant metastasis in the liver and lung of mice after treatment with CPDDs (Supporting Information Fig. S6), implying CPDDs could penetrate into distal lymph nodes, disaggregate and eliminate CTC clusters in the lymphatic circulation. Then, we evaluated the capability of CPDDs to target CTC clusters in blood circulation by CTC clusters metastasis model. Many CTC clusters metastasized to different organs, especially the lungs<sup>38</sup>. A large number of metastatic nodules were observed in the control group. The relative metastatic nodules of the CPDDs, CPDDs and CPDDs groups were 61.5%, 18.7% and 2.5% of the control group, respectively (Fig. 6C and D). The results showed that CPDDs have great potential to inhibit CTC clusters in the blood and lymphatic circulation.

## 4. Conclusions

In this study, we successfully developed cancer-specific calcium nanoregulators for anti-metastasis treatment via modulation of cell–cell interactions. CPDDs had homologous targeting effect, and specifically recognized orthotopic tumor and CTC clusters in the blood and lymphatic circulation. Simultaneously, CPDDs could accumulate intracellular Ca<sup>2+</sup>, effectively disaggregating CTC clusters and inducing mitochondrial-mediated apoptosis pathway, and inhibit the EMT phenomenon, all of which resulted in suppression of the generation and circulation of CTC clusters. Thus, CPDDs showed a significant anti-tumor and anti-metastasis

efficacy, not only in the orthotopic tumor models, but also in the lymphatic and CTC clusters metastasis models. Our findings provide novel insights into anti-metastasis combinational chemotherapy.

## Acknowledgments

This work was supported by National Natural Science Foundation of China (No. 81773656); Liaoning Revitalization Talents Program (No. XLYC1808017, China) and Shenyang Youth Science and Technology Innovation Talents Program (No. RC190454, China).

## Author contributions

Dan Li, Jin Sun and Zhonggui He designed the research. Dan Li, Chang Li and Yingli Wang carried out the experiments and performed data analysis. Haotian Zhang and Qiu Wang participated part of the experiments. Dan Li, Bingjun Sun and Jin Sun wrote the manuscript. Dan Li, Bingjun Sun and Jin Sun revised the manuscript. All of the authors have read and approved the final manuscript.

## Conflicts of interest

The authors have no conflicts of interest to declare.

## Appendix A. Supporting information

Supporting data to this article can be found online at <https://doi.org/10.1016/j.apsb.2021.04.009>.

## References

1. Siegel RL, Miller KD, Jemal A. Cancer statistics 2020. *CA Cancer J Clin* 2020;**70**:7–30.
2. He QJ, Guo SR, Qian ZY, Chen XY. Development of individualized anti-metastasis strategies by engineering nanomedicines. *Chem Soc Rev* 2015;**44**:6258–86.
3. Zhang W, Wang F, Hu C, Zhou Y, Gao HL, Hu J. The progress and perspective of nanoparticle-enabled tumor metastasis treatment. *Acta Pharm Sin B* 2020;**10**:2037–53.
4. Karagiannis GS, Pastoriza JM, Wang YR, Harney AS, Entenberg D, Pignatelli J, et al. Neoadjuvant chemotherapy induces breast cancer metastasis through a TMEM-mediated mechanism. *Sci Transl Med* 2017;**9**.
5. Chang YS, Jalgaonkar SP, Middleton JD, Hai T. Stress-inducible gene *Atf3* in the noncancer host cells contributes to chemotherapy-exacerbated breast cancer metastasis. *Proc Natl Acad Sci U S A* 2017;**114**:7159–68.
6. Keklikoglou I, Cianciaruso C, Guc E, Squadrito ML, Spring LM, Tazzyman S, et al. Chemotherapy elicits pro-metastatic extracellular vesicles in breast cancer models. *Nat Cell Biol* 2019;**21**:190–202.
7. Cheung KJ, Ewald AJ. A collective route to metastasis: seeding by tumor cell clusters. *Science* 2016;**352**:167–9.
8. Aceto N, Bardia A, Miyamoto DT, Donaldson MC, Wittner BS, Spencer JA, et al. Circulating tumor cell clusters are oligoclonal precursors of breast cancer metastasis. *Cell* 2014;**158**:1110–22.
9. Lolas G, Jensen L, Bourant GC, Tsikouritoudi V, Syrigos K. Modeling proteolytically driven tumor lymphangiogenesis. *Adv Exp Med Biol* 2016;**936**:107–36.
10. Gkoutela S, Castro-Giner F, Szczerba BM, Vetter M, Landin J, Scherrer R, et al. Circulating tumor cell clustering shapes DNA methylation to enable metastasis seeding. *Cell* 2019;**176**:98–112.

11. Wang YY, Ma Q, Zhang SL, Liu HY, Zhao BQ, Du B, et al. Digoxin enhances the anticancer effect on non-small cell lung cancer while reducing the cardiotoxicity of adriamycin. *Front Pharmacol* 2020;**11**:186.
12. Schneider NFZ, Cerella C, Simões CMO, Diederich M. Anticancer and immunogenic properties of cardiac glycosides. *Molecules* 2017;**22**:1932.
13. Joseph JV, Conroy S, Pavlov K, Sontakke P, Tomar T, Eggens-Meijer E, et al. Hypoxia enhances migration and invasion in glioblastoma by promoting a mesenchymal shift mediated by the HIF1 $\alpha$ -ZEB1 axis. *Cancer Lett* 2015;**359**:107–16.
14. Khajah MA, Mathew PM, Luqmani YA. Na<sup>+</sup>/K<sup>+</sup> ATPase activity promotes invasion of endocrine resistant breast cancer cells. *PLoS ONE* 2018;**13**:0193779.
15. Ye H, Wang KY, Lu Q, Zhao J, Wang ML, Kan QM, et al. Nanosponges of circulating tumor-derived exosomes for breast cancer metastasis inhibition. *Biomaterials* 2020;**242**:119932.
16. Ye H, Wang KY, Wang ML, Liu RZ, Song H, Li N, et al. Bioinspired nanoplatelets for chemo-photothermal therapy of breast cancer metastasis inhibition. *Biomaterials* 2019;**206**:1–12.
17. Sun HP, Su JH, Meng QS, Yin Q, Chen LL, Gu WW, et al. Cancer-cell-biomimetic nanoparticles for targeted therapy of homotypic tumors. *Adv Mater* 2016;**28**:9581–8.
18. Fang RH, Kroll AV, Gao WW, Zhang LF. Cell membrane coating nanotechnology. *Adv Mater* 2018;**30**:1706759.
19. Zhu YF, Yu XR, Thamphiwatana SD, Zheng Y, Pang ZQ. Nanomedicines modulating tumor immunosuppressive cells to enhance cancer immunotherapy. *Acta Pharm Sin B* 2020;**10**:2054–74.
20. Kroll AV, Fang RH, Jiang Y, Zhou JR, Wei XL, Yu CL, et al. Nanoparticulate delivery of cancer cell membrane elicits multiantigenic antitumor immunity. *Adv Mater* 2017;**29**.
21. Wei RR, Sun DN, Yang H, Yan J, Zhang X, Zheng XL, et al. CTC clusters induced by heparanase enhance breast cancer metastasis. *Acta Pharmacol Sin* 2018;**39**:1326–37.
22. Zhang WJ, Song SC, Wang HX, Wang Q, Li D, Zheng SZ, et al. *In vivo* irreversible albumin-binding near-infrared dye conjugate as a naked-eye and fluorescence dual-mode imaging agent for lymph node tumor metastasis diagnosis. *Biomaterials* 2019;**217**:119279.
23. Cao HQ, Dan ZL, He XY, Zhang ZW, Yu HJ, Yin Q, et al. Liposomes coated with isolated macrophage membrane can target lung metastasis of breast cancer. *ACS Nano* 2016;**10**:7738–48.
24. Zhao QC, Barclay M, Hilken J, Guo XL, Barrow H, Rhodes JM, et al. Interaction between circulating galectin-3 and cancer-associated MUC1 enhances tumour cell homotypic aggregation and prevents anoikis. *Mol Cancer* 2010;**9**:154.
25. Reticker-Flynn NE, Bhatia SN. Aberrant glycosylation promotes lung cancer metastasis through adhesion to galectins in the metastatic niche. *Cancer Discov* 2015;**5**:168–81.
26. Liu X, Taftaf R, Kawaguchi M, Chang YF, Chen WJ, Entenberg D, et al. Homophilic CD44 interactions mediate tumor cell aggregation and polyclonal metastasis in patient-derived breast cancer models. *Cancer Discov* 2019;**9**:96–113.
27. Patriarca C, Macchi RM, Marschner AK, Mellstedt H. Epithelial cell adhesion molecule expression (CD326) in cancer: a short review. *Cancer Treat Rev* 2012;**38**:68–75.
28. Betancur PA, Abraham BJ, Yiu YY, Willingham SB, Khameneh F, Zarnegar M, et al. A CD47-associated super-enhancer links pro-inflammatory signalling to CD47 upregulation in breast cancer. *Nat Commun* 2017;**8**:14802.
29. Cheng H, Jiang XY, Zheng RR, Zuo SJ, Zhao LP, Fan GL, et al. A biomimetic cascade nanoreactor for tumor targeted starvation therapy-amplified chemotherapy. *Biomaterials* 2019;**195**:75–85.
30. Lv YL, Liu M, Zhang Y, Wang XF, Zhang F, Li F, et al. Cancer cell membrane-biomimetic nanoprobe with two-photon excitation and near-infrared emission for intravital tumor fluorescence imaging. *ACS Nano* 2018;**12**:1350–8.
31. Zhu JY, Zheng DW, Zhang MK, Yu WY, Qiu WX, Hu JJ, et al. Preferential cancer cell self-recognition and tumor self-targeting by coating nanoparticles with homotypic cancer cell membranes. *Nano Lett* 2016;**16**:5895–901.
32. Cao HQ, Zou LL, He B, Zeng LJ, Huang YZ, Yu HJ, et al. Albumin biomimetic nanocorona improves tumor targeting and penetration for synergistic therapy of metastatic breast cancer. *Adv Funct Mater* 2017;**27**:14.
33. He XY, Cao HQ, Wang H, Tan T, Yu HJ, Zhang PC, et al. Inflammatory monocytes loading protease-sensitive nanoparticles enable lung metastasis targeting and intelligent drug release for anti-metastasis therapy. *Nano Lett* 2017;**17**:5546–54.
34. Prassas I, Diamandis EP. Novel therapeutic applications of cardiac glycosides. *Nat Rev Drug Discov* 2008;**7**:926–35.
35. Reddy D, Kumavath R, Barh D, Azevedo V, Ghosh P. Anticancer and antiviral properties of cardiac glycosides: a review to explore the mechanism of actions. *Molecules* 2020;**25**:3596.
36. Yang SC, Liu Y, Li MY, Ng CSH, Yang SL, Wang SS, et al. FDX1 promotes tumor growth and metastasis by activating Wnt/ $\beta$ -catenin signaling pathway and EMT in non-small cell lung cancer. *Mol Cancer* 2017;**16**:124.
37. Xu LH, Tong GH, Song QL, Zhu CY, Zhang HL, Shi JJ, et al. Enhanced intracellular Ca<sup>2+</sup> nanogenerator for tumor-specific synergistic therapy via disruption of mitochondrial Ca<sup>2+</sup> homeostasis and photothermal therapy. *ACS Nano* 2018;**12**:6806–18.
38. Headley MB, Bins A, Nip A, Roberts EW, Looney MR, Gerard A, et al. Visualization of immediate immune responses to pioneer metastatic cells in the lung. *Nature* 2016;**531**:513–7.